An effective procedure for the synthesis of monocrystalline spherical nanoparticles of hematite (α-Fe_2O_3)

(submitted to Journal of Nanoparticle Research)

Introduction

Fe_2O_3 nanoparticles present novel physical and chemical properties in comparison to the bulk materials. These novel properties confer potential interesting applications in catalysis, magnetic recording media, pigments, anticorrosive agents and gas sensors [1-5]. In recent years, different methods, such as ball-milling [6], sol-gel technique [7], microemulsion method [8], a combination of both [9], microwave method [10], hydrothermal

Procedure [11], chemical precipitation [12], have been successfully used to synthesize Fe_2O_3 nanoparticles. Among the previously mentioned methods, chemical precipitation is relatively the simplest and less costly synthesis procedure. Moreover, the size control becomes easy by altering parameters, like concentration, pH or calcination temperature.

Goethite (α-FeOOH), ferrihydrite (Fe5H8.4H2O) and akaganeite (β-FeOOH) are the oxyhydroxides, which are obtained by precipitation from the addition of an alkaline solution to an iron-ionic solution. Akaganeite needs the presence of large ions, such as chloride, for the formation of its tunnelling structure [13]. A moderate thermal treatment of these oxyhydroxides normally leads to crystalline α-Fe2O3, which is the most thermodynamically stable phase.

In this work, akaganeite and monocrystalline nanoparticles α-Fe2O3, which result from the thermal treatment of akaganeite, are synthesized through a simple chemical precipitation procedure. Its chemical, textural and morphological properties are determined, compared and discussed by powder X-Ray Diffraction, B.E.T surface area analysis, TEM and SEM microscopies and Temperature Programmed Reduction/Oxidation (TPR/O).

Experimental

Fe_2O_3 by chemical precipitation ($Fe_2O_{3,\ syn}$)

The precipitation of iron oxyhydroxides species with subsequent heating at 350 °C was used to prepare an iron oxide based material. An aqueous solution (1L) of $FeCl_3$ (0.012 M) was stirred at room temperature. Then, an aqueous solution of $(NH_4)_2CO_3$ (0.3 M) was added (≈1 mL/min) drop-wise until a pH value of 7.7 was achieved. After 30 minutes of continuous stirring at 700 rpm and room temperature, the mixture was filtered under vacuum. The solid was washed with MilliQ water until negative chloride test was obtained. The product was dried at 80 °C for 30 minutes and calcined for 2 hours at 350 °C. The precipitation of iron oxyhydroxides species with subsequent heating at 350 °C was used to prepare the synthetic iron oxide based material. After calcination a dark brown-black material was obtained.

β-FeOOH (akaganeite*)*

The procedure to synthesize this material was the same as the one followed in the synthesis of $Fe_2O_{3,syn}$, except for the calcination temperature (60°C). An orange solid was obtained.

Powder X-ray diffraction patterns of the samples were collected in a Siemens D5000 diffractometer with Bragg–Brentano geometry using nickel-filtered Cu-Kα radiation (λ= 0.1541 nm). Data were collected in the 2θ range of 10-70 degrees with an angular step of 0.058 at 3 s per step.

N_2 adsorption and desorption isotherms at 77 K were measured on a Micromeritics ASAP 2000 surface analyzer. Before analysis, $Fe_2O_{3,syn}$ was degassed in vacuum at 120 °C for 16 h. Analogously, akaganeite was degassed in vacuum at 60°C for 24h.

Scanning electron microscopy analysis combined with energy dispersive X-ray analysis (SEM–EDX) was carried out in a JEOL JSM6400 scanning microscope operating at an accelerating voltage in the 15–20 kV range. Samples were previously coated with gold by sputtering technique to create contrast.

The morphology and size distribution of the metal particles was investigated by TEM in a JEOL JEM-2000EX II microscope operated at 80 kV. The solid sample, which was homogeneously dispersed in pure acetone by means of an ultrasonic bath, was deposited in the copper grid and then the solvent was allowed to evaporate under vacuum before analysis.

Temperature Programmed Reduction (TPR) measurements were performed using a Thermofinnigan TPDRO 1100 system. A mixture of H_2 (5%) in argon with a flow of 20 mL/min was used to reduce the samples (0.19 g) placed in an oven heated up from 40 °C to 990 °C with a heating rate of 5 °C/min and left at 990 °C for 20 minutes. Temperature Programmed Oxidation (TPO) measurement were performed using the same system and temperature program, but using a mixture of O_2 (5%) in helium.

Results

Powder X-Ray Diffraction (XRD)

The XRD patterns (Fig. 1) confirmed the presence of hematite phase for the sample of $Fe_2O_{3,\ syn}$, prepared as described in the experimental section. The peaks are in good agreement with those of the JCPDS file 33-0664. In the same way, the peaks

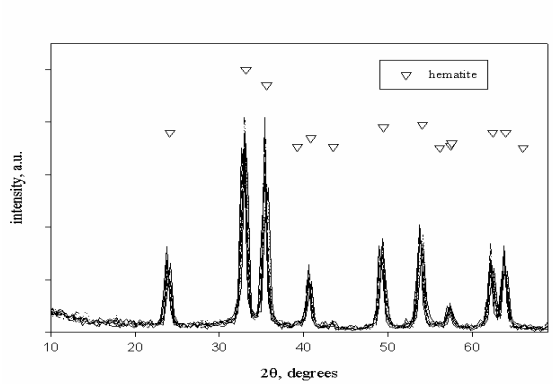

Figure 1 XRD pattern of $Fe_2O_{3,\ syn.}$

of the XRD pattern of the prepared akaganeite were also coincident with those shown by JCPDS file 34-1266 (Fig. 2).

The crystallite sizes of $Fe_2O_{3,\ syn}$ was calculated by the TOPAS version 2.1.using the theory of integral breadth of the diffraction lines (for the peak at $2\theta \approx 35.1530°$) which assumes an intermediate crystallite size broadening modelled by a Voigt [14].

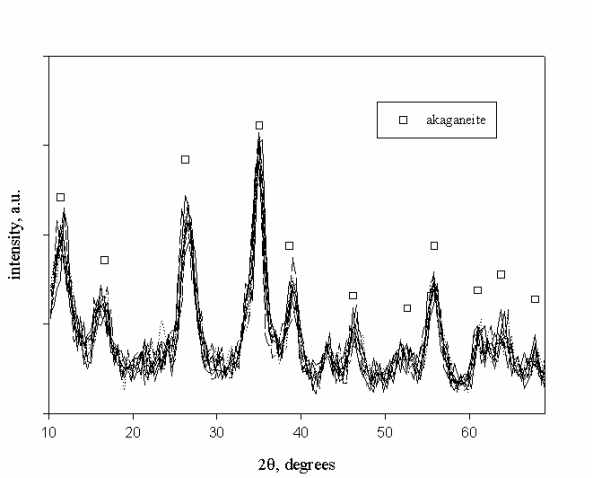

Figure 2 XRD pattern of akaganeite.

The values obtained was 14.88(90) nm (the value in brackets represents the associated error).

Nitrogen physisorption

The isotherm plots of the materials were performed in order to study their textural properties. Both $Fe_2O_{3,\ syn}$ and akaganeite show type IV (Figs. 3, 4), according to the BDDT classification [15]. Their surface area values were 79 and 253 m^2/g, respectively. However, they show different hysteresis loop types (according to IUPAC): $Fe_2O_{3,\ syn}$ isotherm exhibits a hysteresis loop of type H_1, while akaganeite isotherm has a hysteresis loop of type H_2. The pore volume for $Fe_2O_{3,\ syn}$ is 0.27 cm^3/g and for akaganeite is 0.28 cm^3/g.

The pore-size distribution plots, obtained according to the Barrett-Joyner-Halenda (BJH) method are shown in Fig. 5. The predominant pore diameter for akaganeite is around 3.7 nm and for $Fe_2O_{3,syn}$ is 8.8nm, approximately.

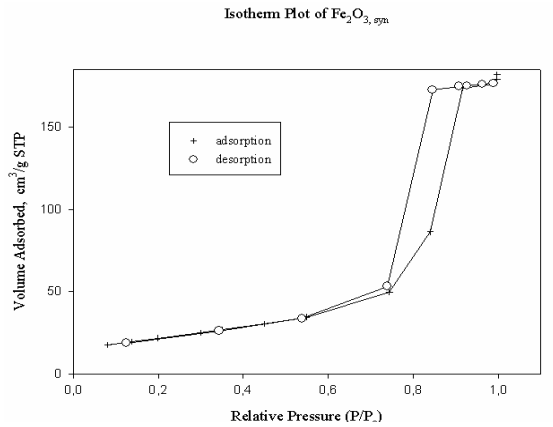

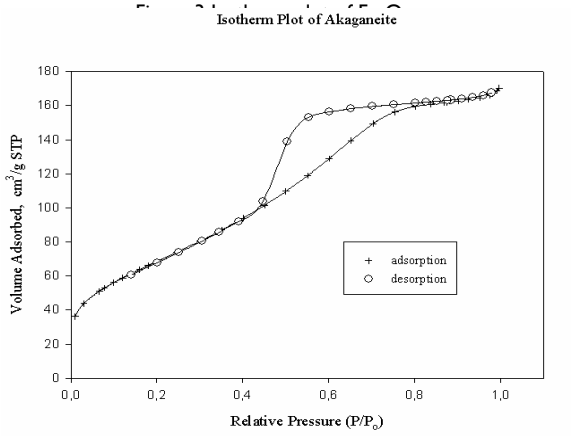

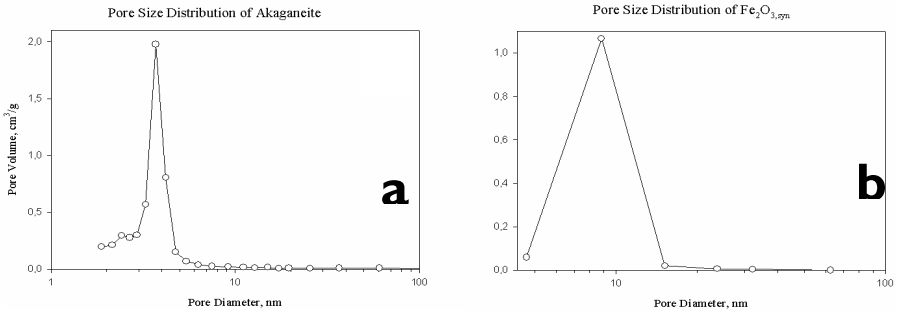

Figure 5 BJH Desorption dV/dlog(D) Pore Volume plot of: a) akaganeite and b)$Fe_2O_{3,syn}$.

Scanning electron microscopy (SEM)

Fig. 6 shows the SEM micrographs obtained from the different samples. Akaganeite micrographs show a low crystalline and non-defined structure with porosity (Fig. 6a and 6b). $Fe_2O_{3,\ syn}$ micrographs (Fig. 6c and 6d) reveal a nanoparticle–aggregated-morphology. The shape of these nanoparticles seems to be spherical, although TEM analyses are required to confirm it.

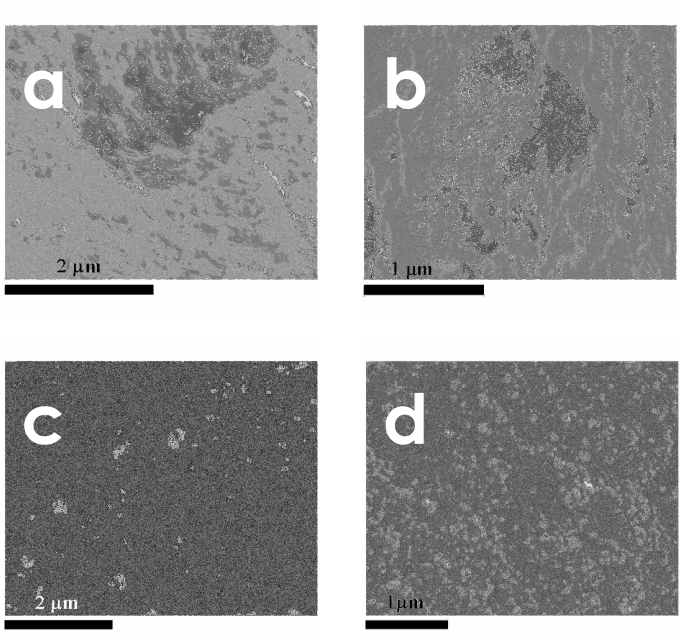

Figure 6 SEM micrographs of the samples. **a** and **b** correspond to akaganeite, **c** and **d** are the obtained images of aggregated $Fe_2O_{3,\ syn}$ nanoparticles.

Transmission electron microscopy (TEM)

In Fig. 7 (a-b), the aggregates of $Fe_2O_{3,\ syn}$ nanoparticles are clearly shown. After the dilution of nanoparticles followed by sonication during not less than 30 minutes, the nanoparticles are disaggregated giving place to clearly separated spherical

nanoparticles with a size distribution shown in Fig. 7c. Around 74 % of nanoparticles have a size between 6 and 14 nm.

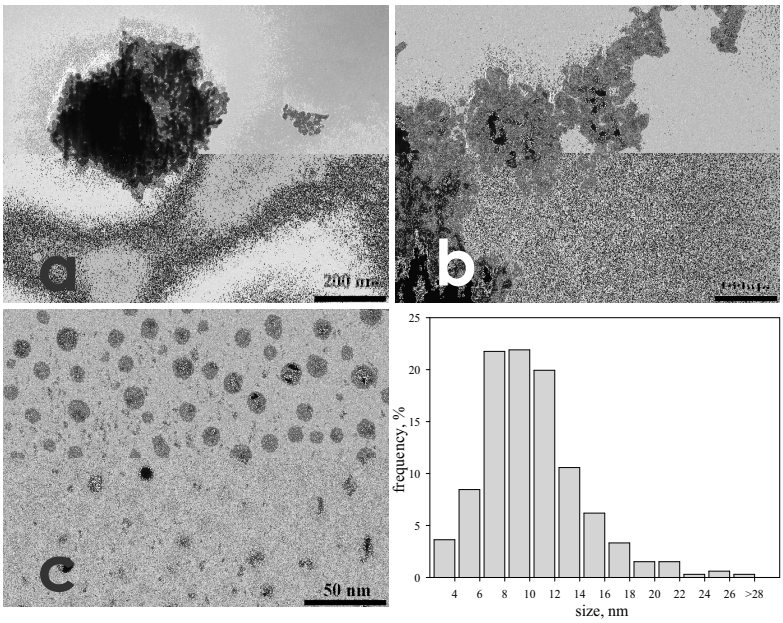

Figure 7 TEM images of $Fe_2O_{3,\ syn}$: **a** and **b** images correspond to an aggregate of nanoparticles, **c** shows more disaggregated spherical nanoparticles. The histogram displays the particle size distribution.

Temperature Programmed Reduction/Oxidation (TPR/TPO)

The capability of the samples to be reduced and oxidized is studied by TPR and TPO. In the case of akaganeite (Fig. 8), two partially overlapped peaks were detected between 210 °C and 430 °C. A defined peak with apparently a shoulder was detected at higher temperature around 700 °C. Between the peak at 430 °C and the peak around 700 °C, the hydrogen kept on being consumed; this may be explained by a reduction process. After the peak around 700 °C, the amount of consumed hydrogen continued increasing. TPO analysis (dotted line) showed only one clear wide peak centred around 700 °C. The second reduction (dashed line) showed two peaks again, at 540 °C and at 720 °C.

The first TPR (solid line) of $Fe_2O_{3,\ syn}$ (Fig. 9) presented three clear overlapped peaks with increasing intensity between 200 °C and 450 °C. A second marked peak around 700 °C was also present. The oxidation process showed a much smoothed peak around 700 °C. The profile for its second reduction process was similar to

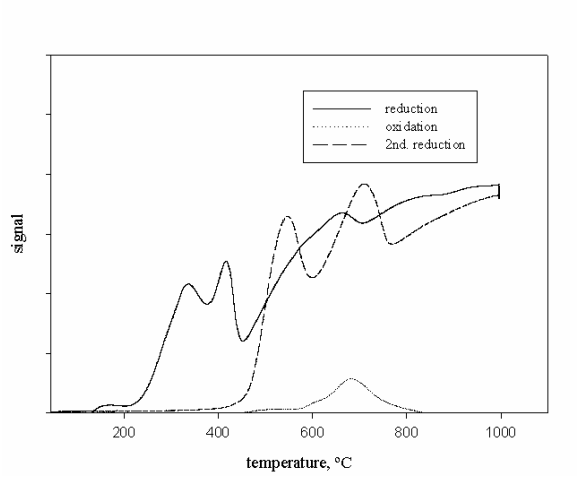

Figure 8 TPR and TPO measurements of akaganeite.

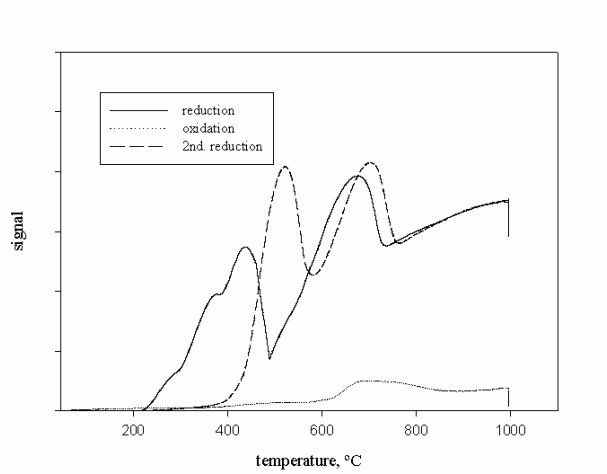

Figure 9 TPR and TPO measurements of $Fe_2O_{3,\ syn}$.

that shown in the measurement of akaganeite.

Discussion

The peaks of the XRD pattern of $Fe_2O_{3,\ syn.}$ match completely those from crystalline α-Fe_2O_3 phase. Concerning the synthesized akaganeite XRD pattern, it also exhibits one single phase of akaganeite. Nevertheless, the broadening of the peaks may be attributed to the low crystallinity of the material or to the low particle size. The calculated crystallite size of $Fe_2O_{3,syn.}$ is similar to that measured in TEM images, which suggests the obtaining of monocrystalline particles.

The profile of $Fe_2O_{3,syn}$ isotherm (Type IV with a hysteresis loop of Type H1) is typical of mesoporous containing materials. Type H1 hysteresis loops are typical for adsorbents with well-defined structures and narrow pore-size distributions. Its mesoporosity is also observed in the predominant pore diameter at the particle size distribution plot (Fig. 7). The surface area of these hematite nanoparticles is lower than expected maybe due to particle-to-particle junctions.

The high surface area (258 m^2/g) of akaganeite may be attributed to its porosity and its large pore volume value. As in the previous case of $Fe_2O_{3,\ syn}$, a Type IV-isotherm plot has been obtained. However, the hysteresis loop is classified as Type H_2, which is typically presented for wormhole-structured materials [16]. The presence of H_2-type hysteresis indicates that the effective radii of the mesoporous bodies are inhomogeneously distributed and the effective radii of the narrow entrance are of equal size. The H_2-type of the hysteresis loop is typical of wormhole-structured materials [16].

To our knowledge, the α-Fe_2O_3 nanoparticles described in the literature so far have not been obtained using the above-described process [6, 9, 2]. Critical procedure parameters such as concentrations and pH values allowed us to obtain α-Fe_2O_3 nanoparticles unlike a previously described procedure [17]. This fact confirms that the morphology and microstructure of hematite particles are strongly dependent on the preparation method and on the specific synthesis conditions.

Fe_2O_3 particles trend to aggregate as it is shown in SEM (Figs. 6c, 6d) and in TEM (Figs. 7a, 7b) analyses. Although the dark colour of $Fe_2O_{3,\ syn}$ could suggest the presence of magnetite, the material presented no magnetic properties. Besides,

sonicated samples prepared for TEM measurements provided an intense orange-red colour, typical of Fe_2O_3-based materials, indicating desegregation.

Regarding the reactivity of Fe_2O_3 under reductive conditions, it is well known that the reduction of bulk iron oxide by hydrogen proceeds through the following steps [18, 19]:

$$Fe_2O_3 \xrightarrow{H_2} Fe_3O_4 \xrightarrow{H_2} FeO \xrightarrow{H_2} Fe$$

If all reduction steps were about to be clearly detected by TPR, three peaks should be observed. We need combining TPR/TPO/TPR (Figs. 8, 9) profiles in order to assign the peaks to the phases. Concerning TPR/TPO analyses of akaganeite (Fig. 8), the solid line shows an ascending profile with three maxima. The high temperature reached in the oxidation process (dotted line) ensures the conversion of Fe to α-Fe_2O_3. The second reduction (dashed line) performed immediately after oxidation exhibits two clear maxima and a positive-slope profile from 800 °C to 990 °C. The presence of two defined peaks may facilitate their assignation to the reduction steps: the peak centred at 540 °C is attributed to $Fe_2O_3 \rightarrow Fe_3O_4$ and the peak at 720 °C is assigned to $Fe_3O_4 \rightarrow FeO$. The slight differences with reported values are presumably due to different experimental conditions, such as the heating rate [20]. The positive slope of the profile during the whole process, even at 990 °C, indicates that a reduction process still occurs; thus the conversion of the starting oxide towards Fe is not totally completed.

In the first reduction (solid line), the peaks shown between 210 °C and 430 °C are not assigned to a reduction step, but to the loss of surface hydroxyls and residual chloride. The peak is not detected in the second reduction (dashed line) because hydroxylation process is not expected to occur during oxidation [21]. The absence of defined peaks between 430 °C and 660 °C may suggest the simultaneous presence of the mixed hematite, maghemite, and magnetite phases during the reduction. FeO (wüstite) is probably not present until 570 °C, because it is an unstable oxide below 570 °C as it decomposes to α-Fe and Fe_3O_4 [22]. Around 700 °C, the reduction step may be assigned to $Fe_3O_4 \rightarrow FeO$. A small shift between the peaks assigned to the formation of wüstite between the first (solid line) and second

(dashed line) reduction may be accounted for the loss of surface area because of sample sintering in the thermal treatments.

Concerning TPR/TPO analyses of $Fe_2O_{3,syn}$ (Fig. 9), the first peak closely before 400 °C is again attributed to the loss of surface hydroxyls. It is worth pointing out the possibility that the maximum at 450 °C in the first reduction is caused by the reduction step of $Fe_2O_3 \rightarrow Fe_3O_4$. Again the shift of this peak in the second reduction profile may be produced by the sintering effect of the sample. The peak assigned to the obtaining of wüstite, located around 700 °C, is more defined than in the case of akaganeite. The fact of having more defined peaks is presumably related to the nano-size of hematite particles which favours the formation of one single phase, since the TPR profile obtained from a commercial micro-sized hematite did not show such a clearly defined peak. The rest of the profile may be understood by the previous discussion. The reason of the alike-dotted curves (second reduction) is because the two samples suffered the same reduction/oxidation thermal treatment, and consequently, the same sintering effect.

Conclusions

A procedure based on the chemical precipitation of iron oxyhydroxide from mixing diluted $FeCl_3$ solution and $(NH_4)_2CO_3$ with drying and ulterior thermal treatment at 350 °C for 2 hours has proved to be an effective procedure to obtain hematite nanoparticles. During the formation process of α-Fe_2O_3 nanoparticles, akaganeite (β-FeOOH).is firstly produced through the precipitation of iron oxyhydroxide and ulterior mild thermal treatment at 60°C. When the thermal transformation is performed at 350 °C, then hematite nanoparticles are formed. These hematite nanoparticles show a spherical monocrystalline structure, with a particle size distribution between 6-14 nm. The increase of temperature causes a decrease in the pore size and surface area of the materials with typically mesoporous isotherm plots. Akaganeite and hematite nano-particles presented similar oxidation/reduction properties. Two interesting points may be drawn from this work, the presentation of a simple and effective procedure to synthesize nano- sized hematite and

akaganeite, and the complete structural characterization carried out, including the characterization, unlike previous published works, of the oxidation/reduction properties (TPR/TPO/TPR) of these nano-sized materials, which allowed the study of their reactivity under red-ox conditions. The knowledge of those properties is relevant in applied processes involving oxidation-reduction mechanisms, such as the catalytic styrene synthesis, water-gas shift, etc.

References

[1] Kodama RH, Makholoufand SA, Berkowitz AE. Phys Rev Lett 1997; 79: 1393

[2] Jiang JZ, Lin K, Lin W. J Phys D Appl Phys 1997; 30: 1459

[3] Dimitrov DV, Hadjipanayis GC, Papaefthymiou V. J Magn Magn Mater 1998; 8: 188

[4] Suber L, Fiorani D, Imperatori P. Nanostruct Mater 1999; 11: 797

[5] Liu XQ, Tao SW, Shen YS. Sens Actuators B Chem 1997; 40: 161

[6] Borzi RA, Stewart SJ, Punte G, Mercader RC, Vasquez-Mansilla M, Zysler RD, Cabanillas ED. J Magn Magn Mater 1999; 205: 234

[7] Xu M, Bahl CRH, Frandsen C, Mørup S. J Colloid Interf Sci 2004; 279:132

[8] Bourlinos A, Simopoulos A, Petridis D. Chem Mater 2002; 14: 899

[9] Woo K, Lee HJ. J Magn Magn Mater 2004; 272–276: 1155

[10] Li Q, Wei Y. Mater Res Bull 1998; 33: 779

[11] Giri S, Samanta S, Maji S, Ganguli S, Bhaumik A. J Magn Magn Mater 2005; 285: 296

[12] Fan H, Song B, Liu J, Yang Z, Li Q. Mater Chem Phys 2005; 89: 321

[13] Mackay AL. Min Mag 1960; 32: 545

[14] TOPAS 31 *General profile and structure analysis software for powder diffraction data User's manual*, Bruker AXS GmbH, Karlsruhe, Germany

[15] Sing KSW, Everett DH, Haul RAW, Moscou L, Pietotti RA, Rouquerol J, Siemienieska T. Pure Appl Chem 1985; 57: 603

[16] Srivastava DN, Perkas N, Gedanken A, Felner I. J Phys Chem B 2002; 106: 1878

[17] Deliyanni EA, Bakoyannakis DN, Zouboulis AI, Matis KA, Nalbandian L. Microporous Mesoporous Mater 2001; 42 : 49

[18] Kock AJHM, Fortuin HM, Geus JW. J Catal 1985; 96: 261

[19] Geus JW. Appl Catal 1986; 25: 313

[20] Neri G, Visco AM, Galvagno S, Donato A, Panzalorto M. Thermochim Acta 1999; 329: 39

[21] Ndlela SC, Shanks BH. Ind Eng Chem Res 2003; 42: 2112

[22] Edstrom J. J Iron Steel Inst 1953; 175: 289